Analytical Biochemistry 472 (2015) 7–20

Contents lists available at ScienceDirect

Analytical Biochemistry

journal homepage: www.elsevier.com/locate/yabio

Concomitant Raman spectroscopy and dynamic light scattering for characterization of therapeutic proteins at high concentrations

Chen Zhou [a], Wei Qi [b], E. Neil Lewis [b], John F. Carpenter [a,*]

[a] Department of Pharmaceutical Sciences, University of Colorado, Anschutz Medical Campus, Aurora, CO 80045, USA
[b] Malvern Instruments, Columbia, MD 21046, USA

ARTICLE INFO

Article history:
Received 15 July 2014
Received in revised form 19 November 2014
Accepted 20 November 2014
Available online 2 December 2014

Keywords:
Protein stability
Aggregation
Raman spectroscopy
Dynamic light scattering
Antibody
Protein formulation

ABSTRACT

A Raman spectrometer and dynamic light scattering system were combined in a single platform (Raman–DLS) to provide concomitant higher order structural and hydrodynamic size data for therapeutic proteins at high concentration. As model therapeutic proteins, we studied human serum albumin (HSA) and intravenous immunoglobulin (IVIG). HSA concentration and temperature interval during heating did not affect the onset temperatures for conformation perturbation or aggregation. The impact of pH on thermal stability of HSA was tested at pHs 3, 5, and 8. Stability was the greatest at pH 8, but distinct unfolding and aggregation behaviors were observed at the different pHs. HSA structural transitions and aggregation kinetics were also studied in real time during isothermal incubations at pH 7. In a forced oxidation study, it was found that hydrogen peroxide (H_2O_2) treatment reduced the thermal stability of HSA. Finally, the structure and thermal stability of IVIG were studied, and a comprehensive characterization of heating-induced structural perturbations and aggregation was obtained. In conclusion, by providing comprehensive data on protein tertiary and secondary structures and hydrodynamic size during real-time heating or isothermal incubation experiments, the Raman–DLS system offers unique physical insights into the properties of high-concentration protein samples.

There are several points during the development history of a therapeutic protein product where there is a need to rapidly assess protein structure, aggregation, and thermal stability. For example, during early development of a therapeutic monoclonal antibody (mAb)[1], relative physical stability (e.g., during heating) and aggregation propensity are often compared among several candidate variants of the antibody [1]. This early testing allows for choice of the variant with the most favorable physical pharmaceutical properties. Similar testing can be performed with the chosen product candidate during pre-formulation studies and formulation development in which the effects of solution conditions such as pH and different excipients on protein unfolding/aggregation are determined [2,3]. These studies are also often conducted under so-called "accelerated degradation" conditions of heating or exposure to other stresses such as forced oxidation. And even after commercial launch of a therapeutic protein, there may be a need to compare its thermal stability and aggregation before and after a manufacturing change [4–6]. Such studies are a vital part of the characterization that is required to provide assurance that the product made by the new manufacturing approach is comparable to the protein made by the original process.

Traditionally for such studies, multiple techniques have been used separately to characterize protein conformation, aggregation, and thermal stability, with the results from different instruments being combined to provide an overall assessment of the protein's physicochemical properties [7]. To characterize size and aggregation, size exclusion chromatography (SEC) is widely and routinely used to quantify the amount of monomer, dimer, trimer, and higher order oligomers [8,9]. Other techniques such as field flow fractionation (FFF) and analytical ultracentrifugation (AUC) are used for orthogonal confirmation of SEC results [10–12]. Dynamic light scattering (DLS), static light scattering (SLS), and turbidity measurements are also used to monitor protein aggregation. For studies of protein structure combined with determination of relative stability (e.g., during heating), optical spectroscopic techniques with varied structural resolution and sensitivity are commonly used, including intrinsic/extrinsic fluorescence, ultravi-

* Corresponding author. Fax: +1 303 724 7266.
E-mail address: john.carpenter@ucdenver.edu (J.F. Carpenter).

[1] *Abbreviations used:* mAb, monoclonal antibody; SEC, size exclusion chromatography; DLS, dynamic light scattering; SLS, static light scattering; UV, ultraviolet; CD, circular dichroism; IR, infrared; HSA, human serum albumin; IVIG, intravenous immunoglobulin; Tyr, tyrosine; Trp, tryptophan; H_2O_2, hydrogen peroxide; PLS, partial least squares; DSC, differential scanning calorimetry; IgG, immunoglobulin G.

http://dx.doi.org/10.1016/j.ab.2014.11.016
0003-2697/

olet (UV) absorbance, far- and near-UV circular dichroism (CD), and infrared (IR) [10,12].

The capacity to perform different measurements in parallel on the same sample is particularly valuable. Often material for studies is limited, especially during the early comparisons between variants of a given mAb product. Obtaining more than one data type from a given sample (e.g., UV absorbance spectra and turbidity measurements, fluorescent spectra and SLS measurements) helps to conserve precious protein. In addition, making simultaneous measurements on a sample ensures that critical solution and processing conditions are identical and that variations in sample handling and instrument operations are minimized.

This consistency is particularly important for real-time studies of protein structure and/or aggregation during heating. Real-time heating studies are useful for relatively rapid characterization of protein stability, but in most cases the protein will aggregate during heating. Because this is an irreversible process, many different factors—such as protein concentration, heating rate, and dwell time at a given temperature for data acquisition—can affect the thermal transition temperatures and, hence, the parameters used to assess relative protein stability. Therefore, often thermal transition temperatures for the same protein obtained on two different instruments will not agree unless extreme care is taken to match all relevant conditions. Sometimes it is not physically possible to obtain the requisite matches between instruments, and then the thermal transition temperatures for different processes, such as protein secondary structural change due to unfolding and protein assembly due to aggregation, cannot be compared rigorously.

The high-concentration formulations used for many modern mAb therapeutics and some older products such as human serum albumin (HSA) and intravenous immunoglobulin (IVIG) make analytical assessment more complicated, even when a single method is used. At the tens of milligrams concentrations found in many of these formulations, certain methods such as fluorescence and far-UV CD spectroscopies might not be viable without sample dilution. Dilution should be avoided in studying protein structure and aggregation because a protein's physical properties and behavior in a dilute solution often do not match those occurring at the actual protein concentration in the product.

In the current study, we addressed these different analytical challenges by using combined parallel measurements of the same sample with Raman spectroscopy and DLS to study the structure, thermal stability, and aggregation of model therapeutic proteins (HSA and IVIG) at high concentrations. DLS, based on the time-dependent correlation of light intensity fluctuation due to Brownian motion of particles, is robust for qualitatively analyzing particle size and sample polydispersity for particle diameters from several nanometers (nm) to a few micrometers (μm). The 173° backscattering detector minimizes interference from multiple scatterings and enables the collection of size distribution data of high-concentration protein samples [10]. Raman spectra provide secondary and tertiary structural information through analysis of peak positions and ratios of spectral features that characterize amide I, amide III, and other backbone vibrations (used to characterize the secondary structure both qualitatively and quantitatively) as well as peaks for vibrations of aromatic side chains such as tyrosine (Tyr) and tryptophan (Trp) (used to monitor protein tertiary structure) [13–17]. Compared with IR spectroscopy, Raman spectroscopy requires minimal sample preparation and is less sensitive to water vibrations that interfere with the amide I band, making it less difficult to subtract this water contribution [18]. Raman spectroscopy is also ideally suited to studying proteins at high concentration [19].

By combining the DLS and Raman spectroscopy systems, we were able to characterize the size distribution and conformation at the same time for the same protein sample. This approach avoids variation issues arising from sample to sample as well as instrumental and experimental conditions. In addition, by acquiring Raman spectra and light scattering data during real-time heating studies and during isothermal incubations at various temperatures, we were able to directly compare the effects of temperature or time of incubation on protein secondary and tertiary structure as well as aggregation.

In our experiments, thermal stability of HSA at pH 7 was first studied to evaluate instrument capability and performance, with varied protein concentrations and heating intervals. Then, the effects of pH (pHs 3, 5, and 8) on HSA conformation, thermal stability, and aggregation were characterized. In addition, during isothermal incubation experiments, HSA aggregation and structural perturbation kinetics were studied at pH 7. As an example of the effects of chemical degradation on protein structure and thermal stability, HSA was oxidized by exposure to hydrogen peroxide (H_2O_2) and the effects on structure, aggregation, and thermal stability were compared with undamaged HSA during real-time heating experiments. Finally, we studied high-concentration formulations of IVIG during real-time heating experiments. Together, these experiments provide insights into the uniquely valuable data that can be obtained with combined study of protein structure, aggregation, and thermal stability with concomitant Raman spectroscopy and DLS.

Materials and methods

Materials

HSA (Albuminar-5, CSL Behring) and IVIG (Gammagard Liquid, Baxter HealthCare) were purchased from the University of Colorado at Boulder's Wardenburg Pharmacy. All other chemicals were purchased from Fisher Scientific (Hampton, NH, USA) and were of reagent grade or higher quality.

Instrument configuration, experimental methods, and data analysis

For the Raman–DLS studies, a Zetasizer Nano ZS (Malvern Instruments, Malvern, UK) was combined with a Kaiser Raman RxN1 spectrometer (Kaiser Optical Systems, Ann Arbor, MI, USA). The instrument is a prototype system developed by the Malvern Bioscience Development Initiative (Columbia, MD, USA). A 785-nm laser with an approximately 280-mW laser power source was used for Raman spectroscopy. DLS data were collected at 632 nm with a 173° backscattering detector that minimizes interference from multiple scatterings and enables the collection of size distribution data of high-concentration protein samples [10]. As shown

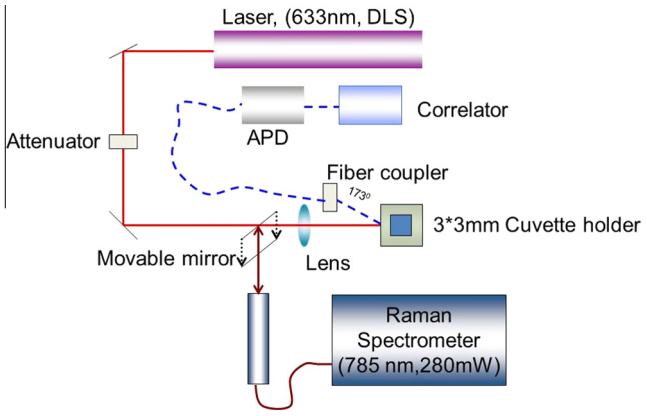

Fig.1. Diagram of the instrument with Raman spectroscopy combined with DLS. APD, avalanche photodiode.

in Fig. 1, a computer-controlled movable mirror enables data collection to be switched between Raman spectroscopy and DLS. In a typical experiment, an approximately 110-μl sample was placed into a 3 × 3-mm quartz cuvette, which was then loaded into a Peltier temperature-controlled sample compartment. To avoid potential problems due to sample evaporation, the sample cuvette was tightly sealed with a Teflon stopper. Unless otherwise noted, Raman spectra were collected with 12 co-additions of a 10-s exposure (see Ref. [20]).

For experiments studying the effects of heating, data were acquired from 20 to 90 °C at 1 °C intervals unless otherwise noted. At each data acquisition temperature, Raman and DLS data were acquired sequentially. Then, the temperature was increased at approximately 6 °C/min to the next data acquisition temperature. The sample was allowed to equilibrate briefly before the data set was acquired and saved, a process that required approximately 4 min. This process was repeated until the experimental temperature range was covered. An automated routine in the software from Malvern was used for the setup and running of the heating experiments; thus, during these runs, operator input and monitoring were not required.

To obtain background Raman spectra for the corresponding buffer without protein, only Raman spectra were acquired during the same temperature ramping and data acquisition protocol. The buffer spectrum at each temperature was subtracted from the spectrum for the protein sample at the same temperature.

Raman spectral data analysis and determination of thermal transition temperatures were performed with a prototype software package provided by the Malvern Biosciences Development Initiative. The Raman spectra midpoint temperature (T_m) and onset temperature (T_{onset}) were calculated by fitting the data with the sigmoidal function:

$$y = \frac{A}{1 + \exp\left(\frac{T_m - x}{B}\right)} + C, \quad (1)$$

where y is the fitted parameter, such as peak center of amide I or contents of α-helix/β-sheet, x is the temperature, and A, B, and C are constants. To obtain the T_{onset} values, the second derivative of the fit was used to find the point of maximum curvature on the rising edge of the transition.

For DLS results obtained during heating experiments, the correlation function data acquired at each temperature were examined. It was observed that there were high-quality fits with relatively low error until sample temperatures well exceeded the onset temperature for an increase in the z-averaged size. For some of these data sets, size distributions were determined and are presented in Results and Discussion. At higher temperatures, the fits were poor because the protein solutions had become gelled and/or grossly precipitated, as assessed by visual observation.

The aggregation onset temperature (T_{agg}) during each heating experiment was determined as the temperature where the z-averaged size exceeded the base value by more than 25%. The base value was calculated as the mean value of the hydrodynamic size at the five initial data points.

In the initial thermal stability study of HSA, the errors for thermal transition values were the results from fitting errors to the data sets for a single sample. For all of the other experiments, T_m, T_{onset}, and T_{agg} errors were for the standard deviations from the means of values obtained for three or more independent samples ($n \geqslant 3$).

Preparation of therapeutic protein samples

HSA was dialyzed in Slide-A-Lyzer Dialysis Cassettes with a 10-kDa molecular weight (MW) cutoff (Pierce, Rockford, IL, USA) against 20 mM sodium phosphate–citrate buffer at 4 °C, with three changes of the external solution, the volume of which exceeded sample volume by 1000-fold. Unless otherwise noted, pH 7 buffer (20 mM sodium phosphate–citrate) was used with 150 mM NaCl. Protein concentration was determined by UV absorbance at 280 nm using an extinction coefficient of 0.53 cm^{-1} ml mg^{-1} [21]. IVIG was used without dialysis in the commercial formulation (250 mM glycine buffer, pH 5). The protein concentration was determined by UV absorbance at 280 nm using an extinction coefficient of 1.357 cm^{-1} ml mg^{-1} [22,23].

Initial thermal stability study of HSA

A dialyzed HSA sample at pH 7 was diluted to a protein concentration of 39 mg/ml. Then, Raman spectra and DLS data were collected during heating from 20 to 90 °C with a data acquisition interval of 1 °C.

Effects of protein concentration and data acquisition interval on HSA thermal stability

To study effects of protein concentration, a dialyzed HSA sample at pH 7 was diluted to 10, 15, 20, and 39 mg/ml. Then, Raman spectra and DLS data were collected during heating of samples at each protein concentration. A data acquisition interval of 1 °C was used.

In a separate study, the effects of data acquisition interval were investigated. HSA (41 mg/ml) was heated from 20 to 90 °C with data acquisition intervals of 0.5, 1, 2, and 5 °C.

Isothermal incubation of HSA

HSA (31 mg/ml) at pH 7 was incubated at 60, 63, and 65 °C. Data were collected from time 0 to approximately 200 min at time intervals of approximately 4 min.

Effects of pH on HSA structure and thermal stability

HSA was dialyzed at 4 °C against 20 mM sodium phosphate–citrate buffer with 150 mM NaCl at three pH values: 3, 5, and 8. After dialysis, it was found that there was a significant amount of insoluble protein aggregates in the pH 3 sample, as assessed visually and by size exclusion chromatography (data not shown). Therefore, the sample was centrifuged at 194,000g for 1 h using an sw55Ti rotor in a Beckman Optima LE-80k ultracentrifuge. The resulting supernatant was used for the experiments. Protein concentration of samples at all three pHs was adjusted to 37 mg/ml. For comparison of effects of pH on structure and HSA size, DLS data and Raman spectra were first obtained at 20 °C. Then, data were acquired at an interval of 1 °C during heating from 20 to 90 °C.

Effects of oxidation with H_2O_2 on HSA structure, aggregation, and thermal stability

HSA (in 20 mM sodium phosphate–citrate buffer at pH 7 with 150 mM NaCl) at a protein concentration of approximately 46 mg/ml was incubated at 37 °C with and without 3% H_2O_2 (v/v) for 5 days. After incubation, the HSA samples that had been incubated with and without H_2O_2 were dialyzed at 4 °C against 20 mM sodium phosphate–citrate buffer (pH 7 with 150 mM NaCl), with three changes of the external solution, the volume of which exceeded sample volume by 1000-fold. Protein concentration was adjusted to 18 mg/ml. For comparison of effects of oxidation on HSA structure and size, DLS data and Raman spectra for oxidized and control samples were first obtained at 20 °C.

The oxidized and control HSA samples were also analyzed by SEC to quantify levels of soluble aggregates. An Agilent 1100 column (Santa Clara, CA, USA) and a Tosoh TSK G3000SWXL column (San Francisco, CA, USA) (7.8 × 300 mm^2) were used. The mobile phase consisted of 100 mM sodium phosphate (pH 7), 100 mM sodium sulfate, and 0.05% (w/v) NaN_3, and the flow rate was 1 ml/min.

Prior to evaluation of the thermal stability of H_2O_2-treated HSA, protein aggregates were removed from the samples by centrifugation at 194,000*g* for 3 h with an sw55Ti rotor in a Beckman Optima LE-80k ultracentrifuge. The control sample, which had not been treated with H_2O_2, was also processed by ultracentrifugation. The protein concentrations in the supernatants of both samples were adjusted to 18 mg/ml. Thermal stability was studied with Raman spectroscopy and DLS during heating from 20 to 90 °C with a heating interval of 1 °C.

Thermal stability of IVIG

To remove any aggregates and particles, IVIG from the product vial was centrifuged at 194,000*g* for 3 h with an sw55Ti rotor in a Beckman Optima LE-80k ultracentrifuge. The resulting supernatant was removed, and the protein was diluted to 51 mg/ml with the IVIG product formulation buffer (0.25 M glycine, pH 5). DLS data and Raman spectra were acquired at an interval of 1 °C during heating from 20 to 90 °C.

Results and discussion

Initial thermal stability study of HSA

The initial study investigated structural transitions and aggregation during heating of a high-concentration (39 mg/ml) solution of HSA. Aggregation was monitored with DLS, and structural transitions were assessed based on temperature-dependent changes in the Raman spectra for the protein. Furthermore, as a relative measure of protein aggregation propensity and thermal stability, temperatures at which there were transitions in measured parameters by either method were calculated and compared.

There are several structural elements in proteins for which bands in the Raman spectrum can be assigned, and such assignments have been made in the literature for HSA [13,15,24–26]. For the HSA spectrum shown in Fig. 2, the peak from around 1650 to 1680 cm^{-1} was assigned to amide I, which results from the protein backbone's C=O stretching coupled with minor contributions from C–N stretching and N–H in-plane bending [18,26]. The amide I band is sensitive to alterations in a protein's secondary structure [13,27]. At 20 °C, the peak position of the amide I band was located at 1653 cm^{-1}, and this band was assigned to α-helix [26,28]. As temperature increased to 65 °C, no significant peak shifting was observed for the amide I band. However, by the time the temperature reached 70 °C, there was peak broadening and a shoulder appeared at 1670 cm^{-1} (Fig. 2). At 80 °C, the peak shifted more toward 1670 cm^{-1}. The amide I peak shifting and broadening during heating were consistent with the gradual loss of α-helix structure and concomitant formation of β-sheet and random coil [24,25,29].

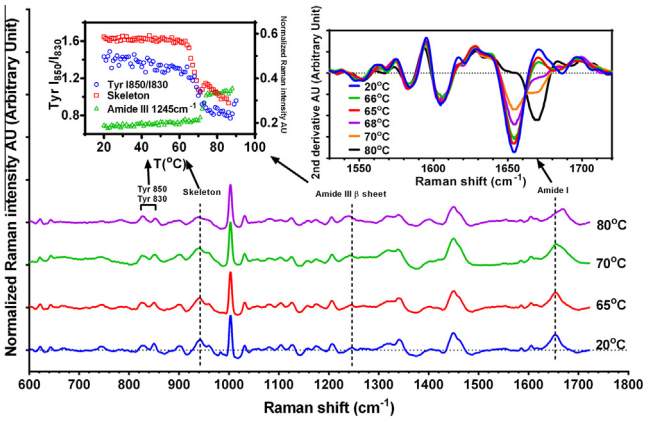

Fig.2. Effects of heating on Raman spectra of HSA and selected spectral elements. HSA was studied at pH 7 and a concentration of 39 mg/ml. The main figure shows Raman spectra with normalized intensities acquired at 20, 65, 70, and 80 °C. The vertical dashed lines were drawn to highlight the change of characteristic Raman bands along with the change of temperature. The upper left inset shows the intensity of the skeleton vibration at approximately 941 cm^{-1} (red rectangles), the amide III band at 1245 cm^{-1} (green triangles), and the intensity ratio of Tyr at 850 and 830 cm^{-1} (blue circles) as a function of temperature. The upper right inset has the second derivative of the amide I region acquired at various temperatures during heating. (For interpretation of the references to color in this figure legend, the reader is referred to the web version of this article.)

To more clearly resolve the component Raman spectral bands within the amide I region and temperature-dependent changes, the second derivative for this region was calculated (Fig. 2, upper right inset). As temperature increased, there was a clear loss of peak intensity at 1653 cm^{-1} that was accompanied by an increase of peak intensity at 1670 cm^{-1}. Thus, as noted above, during heating of HSA, there is a loss of native α-helix and formation of non-native β-sheet and random coil [24,25,29]. An isosbestic point between the two peaks further confirmed the direct transition of native to non-native secondary structural elements in HSA during heating (Fig. 2, upper right inset).

The amide III band at around 1245 cm^{-1}, another indicator for secondary structure, is attributed to the in-plane bending of N–H and stretching of C–N [13,25]. The increased intensity of the 1245-cm^{-1} peak with temperature also can be assigned to the formation of β-sheet structure during heating (Fig. 2, upper left inset).

The Raman band at 941 cm^{-1} (Fig. 2) is usually referred to as the amide skeleton band and results from the N–Cα–C stretching of the peptide backbone [13,27]. For the Raman spectrum of HSA, this band is a marker of α-helix structure [27]. The reduction in intensity at 941 cm^{-1} during heating further confirms the loss of native α-helix structure of HSA.

By monitoring the Fermi doublets at 850 and 830 cm^{-1}, information was obtained about heating-induced changes in HSA's tertiary structure. These spectral features are assigned to the vibrational frequencies of tyrosine, and a change in the intensity ratio of the two peaks (I_{850}/I_{830}) reflects a change in the microenvironment around tyrosine [13,17]. A higher value indicates that the residue is either in a hydrophobic environment or in a polar environment but only moderately hydrogen bonded. In contrast, the value becomes lower if the phenolic hydroxyl oxygen is ionized or becomes a strong hydrogen bond donor [15,17]. Therefore, the decrease of I_{850}/I_{830} for HSA from 1.4 to 0.8 during heating (Fig. 2) suggests that there was a tertiary structural change in which Tyr residues as donors were more strongly hydrogen bonded to a negative-charge receptor such as a carboxylate ion [15,17].

As an example of comparisons that can be made between the heating-induced changes in markers of secondary and tertiary structures, the intensity of the amide skeleton band at 941 cm^{-1} and the values for I_{850}/I_{830} were plotted versus temperature (Fig. 2, upper left inset). For secondary structure, there was not a substantial change until the temperature reached approximately 67 °C, above which there was a relative steep drop in band intensity. Conversely, the tertiary structure as reflected in the values for I_{850}/I_{830} began to be gradually altered as temperature increased above approximately 35 °C and then underwent a more dramatic change starting at approximately 67 °C. Thus, prior to secondary structural transitions, heating leads to perturbation of tertiary structure, and then at higher temperatures it appears that secondary structural changes result in further tertiary structural alterations.

To assess quantitatively heating-induced changes in HSA secondary structure, the Raman spectra were analyzed with two different approaches. In the first, from the second derivative spectra in the amide I region, the intensities were determined for the α-

helix band at 1653 cm^{-1} and the β-sheet band at 1670 cm^{-1}. The values were plotted versus temperature, and curves were fit to the resulting plots (see Materials and Methods for details). Based on the fit curves, T_{onset} and T_m values were determined (Fig. 3A). For the α-helix band, these were 67.0 ± 0.2 and 68.1 ± 0.4 °C, respectively. For the β-sheet band, the corresponding values were 66.0 ± 0.2 and 69.5 ± 0.2 °C. Therefore, the thermal transitions for loss of α-helix band intensity and the gain in β-sheet occurred at essentially the same temperatures. This observation was consistent with the conclusion that during heating of HSA there was a direct conversion of α-helix to β-sheet.

In the second approach, a database provided by Malvern contained Raman spectra of 18 proteins with known secondary structure contents. In addition, a partial least squares (PLS) analysis routine for this spectral database was developed by Malvern. Based on PLS analysis of the HSA spectrum, at 20 °C the protein contained 68% α-helix and 0% β-sheet, which matches well with values obtained by X-ray crystallography [30]. The percentages of α-helix and β-sheet were then plotted versus temperature, and curves were fit to the plots using a sigmoidal model as described in Materials and Methods (Fig. 3A). Based on the fit curves, T_{onset} and T_m values were determined. For the α-helix content, these were 67.0 ± 0.1 and 70.2 ± 0.2 °C, respectively. For the β-sheet content, the corresponding values were 67.0 ± 0.2 and 70.3 ± 0.2 °C. Therefore, with both methods of determining thermal transition temperatures, consistent values were obtained and the results documented that loss of α-helix in HSA during heating was concomitant with an increase in β-sheet content.

The underlying cause of this structural conversion was revealed by examining the DLS data (Fig. 3B) for HSA that were obtained during the same heating experiments as the Raman spectra. At 20 °C, the *z*-averaged hydrodynamic diameter was 7.3 nm, which is consistent with values for HSA in the literature [31]. At 20 °C, the intensity distribution was monodispersed and it remained this way during heating until 63 °C, at which point a peak with approximately 200 nm size was observed, indicating the onset of heating-induced of aggregation (Fig. 3B). At 65 and 70 °C a peak for intermediate-sized aggregates was observed, and at 70 °C there was an additional peak centered around 400 nm. At temperatures higher than 74 °C, the sample was visually observed to be grossly precipitated and the fits to the correlation function data were relatively poor. Thus, size distributions could not be determined above this temperature.

The *z*-average values for HSA size were plotted as a function of temperature. As heating progressed to 62 °C there was no observable change, but above this temperature there was a large increase. A curve was fit to the plot of values versus temperature, and the T_{agg} value was determined (Fig. 3C). The T_{agg} value was lower than T_{onset} for secondary structural changes (63.5 vs. ~66 °C). The discrepancy is probably due to the fact that DLS is very sensitive to large particles because the scattering intensity is proportional to the sixth power of the particle diameter. Thus, the size measured will be skewed to a larger value when even a minute amount of large aggregates is present, that is, less than 1% in mass. With Raman spectroscopy, like all of the other spectroscopic techniques, the spectra represent the average structure of all sub-populations

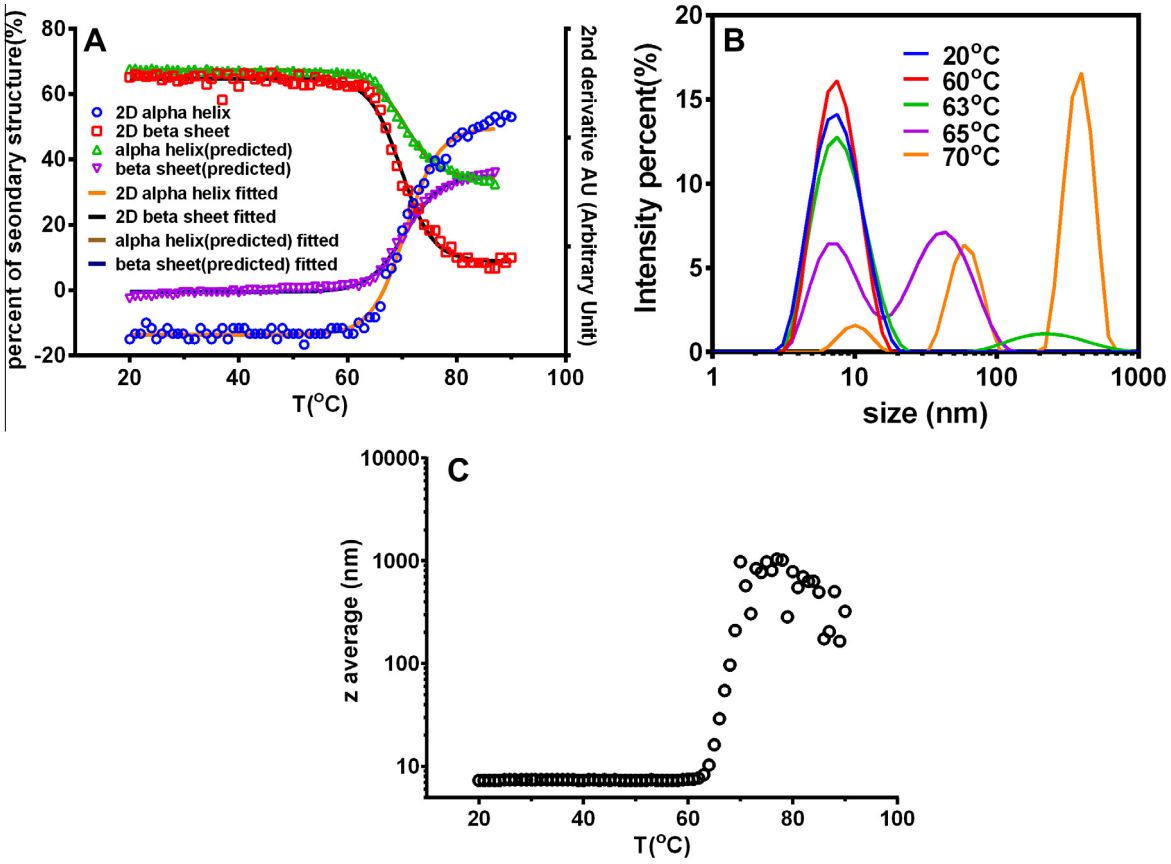

Fig.3. (A) Two ways to characterize the alteration of secondary structure occurring during heating of HSA. In the first approach, the percentages of α-helix and β-sheet were calculated from the Raman spectra using a PLS model as described in Materials and Methods. In the second approach, the relative intensities of the α-helix and β-sheet bands in the second-derivative (2D in the legend) spectra were plotted. The solid lines shown are those resulting from sigmoidal fitting of the data points used for each plot. (B) DLS measured intensity distributions for HSA obtained during heating shown for selected temperatures. (C) The *z*-averaged hydrodynamic size of HSA (39 mg/ml) versus temperature.

and are not sensitive to relatively small amounts of structurally perturbed protein molecules. Thus, even though conversion of a few percentage points of HSA molecules into large aggregates would have a large effect on DLS *z*-average values, the corresponding Raman spectra would not be detectably altered from those observed for the fully native protein.

Overall, the data from Raman spectroscopy and DLS showed that during heating of HSA the first detectable change was perturbation of tertiary structure. As the temperature increased further, the protein aggregated and it was the process of aggregation that caused the loss of native α-helix and the concomitant increase in non-native intermolecular β-sheet. This conclusion is consistent with the commonly found phenomenon that during heating partial unfolding of native structure results in protein aggregation, which in turn is associated with a loss of native secondary structure and formation of intermolecular β-sheet [18,32–35]. These results show the importance of having an independent, but concomitant measure of protein aggregation when studying heating-induced structural transitions of proteins.

Effects of protein concentration and data acquisition interval on HSA thermal stability

To assess the effect of protein concentration on HSA thermal stability, samples of 10, 15, 20, and 39 mg/ml were analyzed at pH 7. At 20 °C, there were no detectable differences between the Raman spectra of HSA at the different concentrations (see Fig. S1 in online Supplementary material). However, the spectral quality increased in direct proportion to the protein concentration. During heating, the peak centers of amide I spectra for HSA at all concentrations studied increased from around 1653 to 1661 cm^{-1}. The T_{onset} and T_m values calculated from the sigmoidal fitting of the temperature-dependent position of amide I are shown in Table 1. Based on both values, under the conditions of our experiments, protein concentration did not affect the stability of HSA during heating (Table 1).

The T_{agg} values obtained from the temperature-dependent *z*-averaged hydrodynamic size also did not vary with protein concentration (Table 1). However, the greater the protein concentration was, the larger the *z*-averaged size was for the sample after the aggregation onset (Fig. 4B, inset). More specifically, at 67 °C, the HSA sample at 10 mg/ml showed two unresolved peaks with *z*-averaged size of 18 nm, whereas for the sample at 39 mg/ml two peaks at 10 and 100 nm were well resolved with *z*-averaged size of 55 nm.

Table 1
Onset and midpoint temperatures for structural changes and aggregation onset during heating.

Experimental parameter tested	T_{onset} (°C)	T_m (°C)	T_{agg} (°C)
HSA concentration			
10 mg/ml	65.8 ± 0.9	71.0 ± 1.4	65.0 ± 0.5
15 mg/ml	65.4 ± 0.6	69.5 ± 0.4	64.8 ± 0.1
20 mg/ml	66.0 ± 0.0	70.4 ± 0.7	64.8 ± 0.6
39 mg/ml	66.7 ± 0.6	70.7 ± 0.7	64.4 ± 0.6
Heating increment for HSA solution			
0.5 °C/step	65.2 ± 0.8	70.1 ± 0.4	62.6 ± 0.2
1 °C/step	65.0 ± 0.0	69.9 ± 0.1	63.3 ± 0.3
2 °C/step	65.2 ± 0.2	70.0 ± 0.2	64.1 ± 0.2
5 °C/step	65.3 ± 0.2	70.4 ± 0.3	64.0 ± 1.7
pH of HSA solution			
pH 3	49.3 ± 0.6	58.9 ± 0.4	45.7 ± 0.9
pH 5	63.3 ± 0.6	66.5 ± 0.3	54.8 ± 0.5
pH 8	65.0 ± 0.0	69.4 ± 0.2	61.8 ± 0.3
H_2O_2-induced HSA oxidation			
Untreated HSA	66.0 ± 1.2	70.2 ± 0.8	57.0 ± 1.9
H_2O_2-treated HSA	58.0 ± 1.2	68.0 ± 0.5	64.4 ± 0.1
IVIG aromatic side chain			
Tyr 830 cm^{-1}	61.0 ± 1.4	68.0 ± 1.7	N/D
Tyr 850 cm^{-1}	60.0 ± 0.8	66.0 ± 1.7	N/D
Trp 1550 cm^{-1}	59.0 ± 2.8	69.0 ± 2.5	N/D
Trp 1340/1360 cm^{-1}	62.7 ± 1.2	68.1 ± 0.9	N/D

The heating step is an operational parameter that can potentially affect thermal stability evaluations for proteins. To gain insight into the effects of heating step interval on protein thermal stability, HSA at 41 mg/ml was evaluated with a heating interval of 0.5, 1, 2, or 5 °C. There were no discernible differences in the heating-induced shifts in the amide I band (Fig. 5A) or in the calculated values for T_{onset} and T_m (Table 1). Temperature-dependent DLS data (Fig. 5B and Table 1) showed that the T_{agg} values also were not affected by heating interval. But the sizes of aggregates obtained were slightly larger for samples studied in experiments with the smaller heating intervals than for those observed with larger intervals (Fig. 5B, inset). This effect was probably because the sample was exposed to higher temperatures for a longer time during the experiments with the smaller data acquisition intervals.

Isothermal incubation of HSA

The kinetics of structural alterations and aggregation for HSA were evaluated during isothermal incubation at 60, 63, and 65 °C, which were near the onset temperatures for the thermal transitions observed during heating experiments. In Fig. 6A, the Raman amide I band position was plotted against the duration of incubation. At the 20 °C starting point, the values were 1654.3, 1654.3, and 1654.7 cm^{-1} for HSA incubated at 60, 63, and 65 °C, respectively. The shift to higher wave numbers was faster and to a greater degree at 65 °C than that observed at 63 °C; there was almost no change for the amide I peak center at 60 °C. After 200 min of incubation, the amide I peak was centered at 1654.5, 1655.4, and 1656.8 cm^{-1} for 60, 63, and 65 °C, respectively. As a direct reflection of protein secondary structure, the amide I peak shifting indicates the structural perturbation rate and extent were both positively correlated with the temperature. As expected, structure perturbation also positively correlated with the increase of *z*-averaged size (Fig. 6B). With starting points of 7.9, 8.4, and 9.9 nm for HSA incubated at 60, 63, and 65 °C, respectively, the *z*-averaged size increased to 9.9, 34, and 116.5 nm, respectively, after 200 min of isothermal incubation. The protein aggregated the fastest and to the greatest extent at 65 °C.

Notably for the sample incubated at 63 °C, the magnitude of the increase in *z*-averaged size was substantially greater than that of the increase in amide I peak position. As discussed above, conversion of a small fraction of the protein population into larger aggregates could result in a substantial increase in the *z*-average value because of the great increase in light scattering with size. In contrast, even if HSA molecules in the aggregates had greatly perturbed secondary structure, with a relatively small fraction converted into aggregates, the impact on Raman spectra would be minor. This is because under these conditions the overall average secondary structure of all protein molecules in the sample would be only slightly altered.

Effects of pH on HSA structure and thermal stability

The effects of pH on the structure and thermal stability of HSA have been characterized by various techniques such as CD spectroscopy, differential scanning calorimetry (DSC), and fluorescence spectroscopy, but the earlier studies were performed at relatively low protein concentrations [21,36–39]. Here, we used the Raman–DLS system to study effects of pH on the structure and thermal stability of HSA at the relatively high concentration of 37 mg/ml. At 20 °C, as compared with the Raman spectra for the

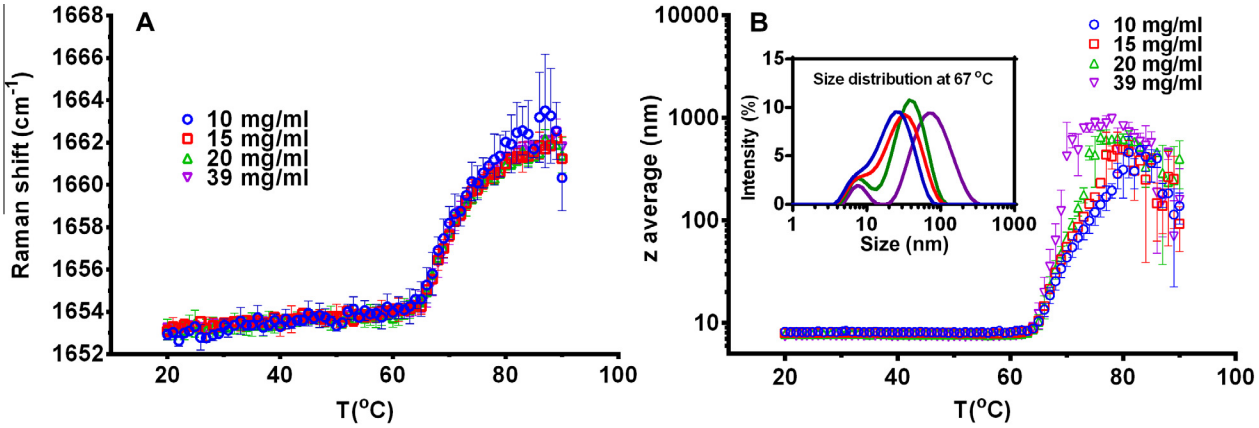

Fig.4. (A) Effect of protein concentration on the Raman spectra amide I peak centers during heating of HSA. The protein was studied (pH 7) at protein concentrations of 10, 15, 20, and 39 mg/ml. (B) Effect of protein concentration on the *z*-averaged hydrodynamic size of HSA during heating. The inset shows the intensity distribution of sizes measured by DLS at 67 °C. Error bars denote standard deviations for values obtained for independent samples ($n \geqslant 2$).

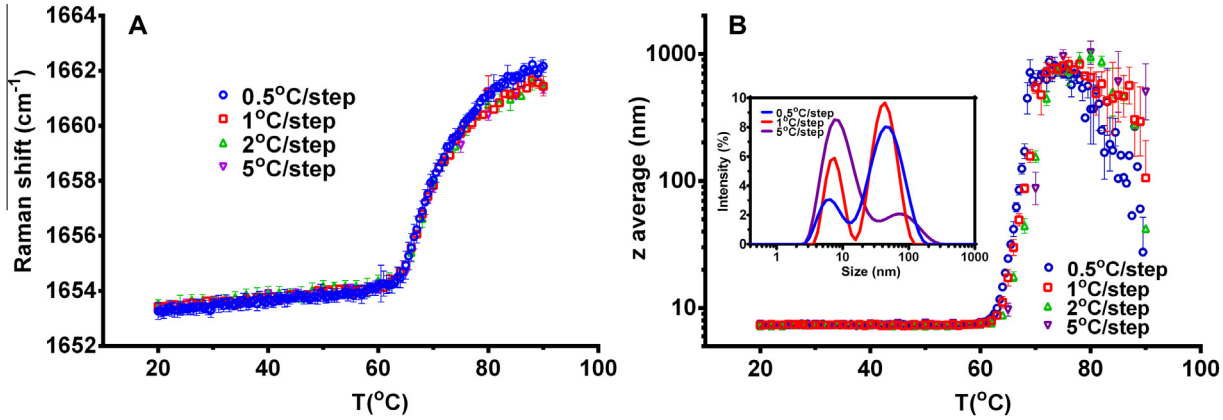

Fig.5. (A) Effect of heating step size on the Raman spectra amide I peak centers during heating of HSA (41 mg/ml). (B) Effect of heating step size on the *z*-averaged hydrodynamic size of HSA during heating. The inset shows the intensity distribution of sizes measured by DLS at 65 °C. Error bars denote standard deviations for values obtained for three independent samples.

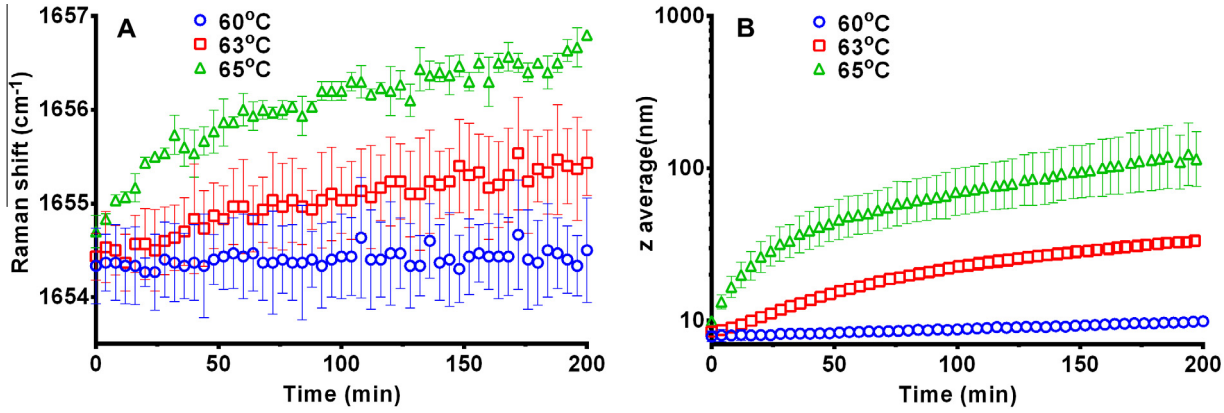

Fig.6. Effect of temperature on Raman spectra amide I peak centers (A) and *z*-averaged hydrodynamic size (B) during isothermal incubation of HSA (31 mg/ml HSA at pH 7). Error bars denote standard deviations for values obtained for three independent samples. In some cases, error bars are not visible because standard deviations were smaller than the symbols.

protein at pH 5 and 8, at pH 3 the second-derivative amide I region showed a slight intensity loss at 1654.5 cm^{-1} and gain at 1670 cm^{-1} (Fig. 7A). This change is attributed to a reduction in α-helix content of HSA at pH 3 [21]. There were also decreases in the intensities at 941 cm^{-1} and at 1320 cm^{-1}, which further confirmed the helical structure decrement (see Fig. S3 in Supplementary material). It has previously been shown that HSA has a compact conformation between pH 4.3 and 10 and converts to a more open structure with reduced helix content—in a process referred to as "acid expansion"—below pH 4.3 [21,36,37]. Consis-

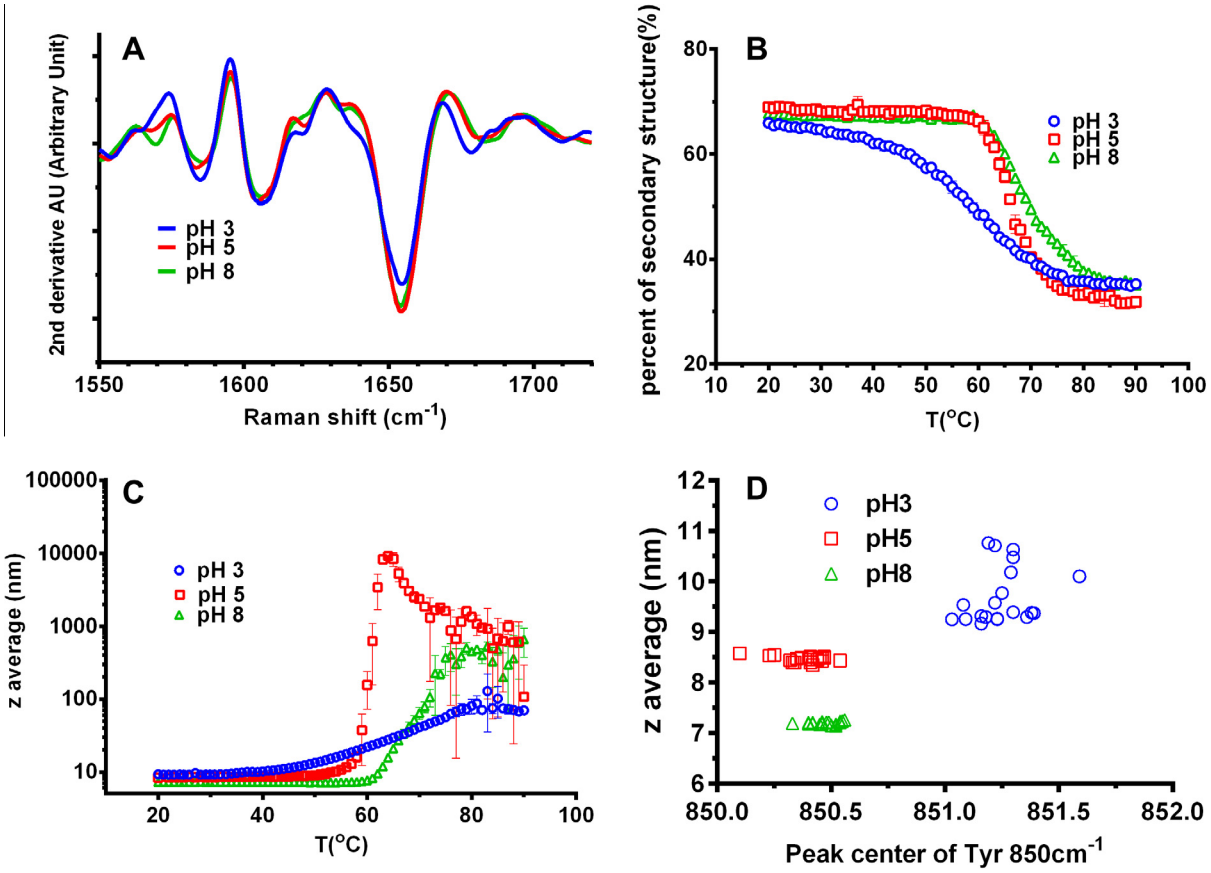

Fig.7. Effect of pH on HSA (37 mg/ml) structure and size. (A) Second derivative of amide I region of the Raman spectra acquired at 20 °C. (B) α-Helix percentage during heating. Helix content was calculated from the Raman spectra as described in Materials and Methods. (C) The *z*-averaged size during heating. (D) The *z*-averaged size and Raman spectra tertiary structure marker, Tyr 850 cm^{-1} band position, at pHs 3, 5, and 8. The first 20 data points from 20 to 39 °C during heating were chosen. In panels B and C, error bars denote standard deviations for values obtained for three independent samples.

tent with this effect of acidic pH on HSA, at 20 °C the *z*-averaged size of HSA was approximately 7, 8, and 9 nm at pHs 8, 5, and 3, respectively.

For the thermal stability study, Raman spectra were collected for HSA samples at each pH from 20 to 90 °C (see Fig. S4 in Supplementary material). For samples at pHs 5 and 8, HSA started with 68% helix content and this value did not change substantially until 65 °C (Fig. 7B). Then, the content dropped relatively steeply with temperature at pH 5 compared with the temperature-induced structural change in HSA observed at pH 8. The HSA sample at pH 3 started with slightly lower helix content (66%) and went through a broader and more gradual temperature-induced transition but with an earlier onset temperature. However, by the point the samples reached 90 °C, HSA helix contents were similar to values of 35, 32, and 35% at pHs 3, 5, and 8, respectively.

The T_{onset} and T_m of secondary structural transitions were determined, and the values of both followed the trend of pH 3 < pH 5 < pH 8 (Table 1). These results demonstrated that HSA thermal stability is substantially reduced at pH 3.

During heating at pH 3, the *z*-averaged size of HSA started at 9 nm (20 °C) and increased gradually with temperature (Fig. 7C). Aggregation was first observed at 45.7 ± 0.9 °C, as evidenced by the increase of the *z*-averaged size to approximately 11 nm. By the time the sample reached 90 °C, the *z*-averaged size was approximately 70 nm. Macroscopically at this point, the sample was visually a transparent diffuse gel. For HSA at pH 5, there was a sharp transition to larger *z*-average size starting at 54.8 ± 0.5 °C, and after heating the aggregated sample had formed a white precipitate. At pH 8 the transition occurred at 61.8 ± 0.3 °C, and during heating the sample formed an opaque gel. For HSA at both pHs, the last size data with correlation coefficient higher than 0.85 indicated a *z*-averaged size of 287.7 nm for pH 5 at 61 °C and 198.2 nm for pH 8 at 74 °C.

The smaller size increase for HSA at pH 3 during heating could be due to highly charged protein molecules and charge–charge repulsion between protein molecules and/or nanoparticles formed during heating. Previously, it has been observed that HSA at pH 2 aggregated less than the protein at pH 7 during heating from 25 to 90 °C [40]. Thus, even though HSA has a perturbed conformation at low pHs, the high positive charge of the molecules limits the magnitude of aggregation during heating; conformational stability of HSA is reduced, but colloidal stability is increased.

Finally, in Fig. 7D, for each pH studied the *z*-averaged size for HSA is plotted against the Tyr 850 cm^{-1} peak center at low temperatures (20–39 °C) where no significant aggregation or denaturation had taken place. It is clear from this plot that HSA at pH 3 has a perturbed tertiary structure and expanded monomer size compared with HSA at pHs 5 and 8. Although the secondary structure differences were small among pHs 3, 5, and 8 (Fig. 7A), the combination of size and tertiary structure marker Tyr 850 cm^{-1} could be used to capture and amplify the small differences in the protein's structure.

Effects of oxidation with H_2O_2 on HSA structure, aggregation, and thermal stability

Oxidation of therapeutic proteins can occur during production in cell cultures due to dissolved oxygen and during downstream

processes. This damage can also occur in the final drug container due to light exposure and/or impurities in excipients and their degradation [41]. Furthermore, often the oxidation of a therapeutic protein causes decreased conformational stability and increased aggregation [41–46]. To evaluate the effects of oxidation on HSA structure and aggregation, we first employed an accelerated degradation approach in which experimental samples were exposed to 3% (v/v) H_2O_2 at 37 °C over 5 days and then analyzed for aggregation by DLS and structural alterations by Raman spectroscopy. SEC was also used to characterize and quantify protein aggregates. Control samples that were incubated at 37 °C without H_2O_2 were similarly analyzed. For the control HSA sample, even after the 5-day incubation, no significant aggregation occurred relative to that found in the starting material, as assessed by both DLS and SEC (see Fig. S5 in Supplementary material). However, for H_2O_2-treated HSA, significant aggregation was observed (Fig. 8). DLS intensity percentage results for the control HSA sample had a monodispersed peak with a center close to 7 nm. In contrast, for the H_2O_2-treated HSA sample, there was an additional prominent peak at 30 nm and the *z*-average size increased greatly (Fig. 8A and C). When DLS results of the H_2O_2-treated HSA were converted to volume percentage for the main peak, there was a tailing in the greater than 10-nm size range, indicating that a fraction of the protein population had aggregated (Fig. 8B). For the control HSA sample, the majority of the protein was monomeric with a minute fraction of high-molecular-weight species. For the H_2O_2-treated sample, as assessed by SEC analysis, there was a substantial decrease in the amount of monomeric HSA and a concomitant increase in high-molecular-weight species (Fig. 8D). Thus, oxidative stress of HSA under accelerated degradation conditions fostered aggregation of the protein, and DLS results plotted as intensity percentage provided a sensitive means by which to detect the aggregates.

In the Raman spectra of the H_2O_2-treated HSA, there was only slight peak shifting and broadening in the amide I region (see Fig. S6 in Supplementary material), which suggests that secondary structure was not significantly altered. Similarly, Raman spectra in the regions of amide I, amide III, and the backbone skeleton bands indicated that the treated HSA did not have observable alterations in secondary structure (data not shown). A recent study also evaluated the effects of H_2O_2 on the structure and aggregation of HSA employing infrared spectroscopy, far-UV CD spectroscopy, and light scattering. It was also found that the secondary structure of HSA was not affected significantly by H_2O_2 treatment [47].

However, differences in the Raman spectra for control and H_2O_2-treated HSA were observed in the 800- to 1300-cm^{-1} region (Fig. 9A). In both the raw spectrum for H_2O_2-treated HSA and the difference spectrum, a new peak at around 1045 cm^{-1} was apparent. This peak has been assigned to SO_2 stretching and was probably due to methionine and/or cystine oxidation [47–50]. However, the oxidation stress employed in our experiment was not as harsh as that described in earlier studies [48,49] where the peracid oxidation of disulfide bridges of the cystine was induced by much higher concentrations of H_2O_2. Therefore, in the spectrum for H_2O_2-treated HSA from our studies, the SO_2 stretching band was more likely due to methionine oxidation, which does not require as harsh treatment conditions as those required for cystine oxidation [47,48].

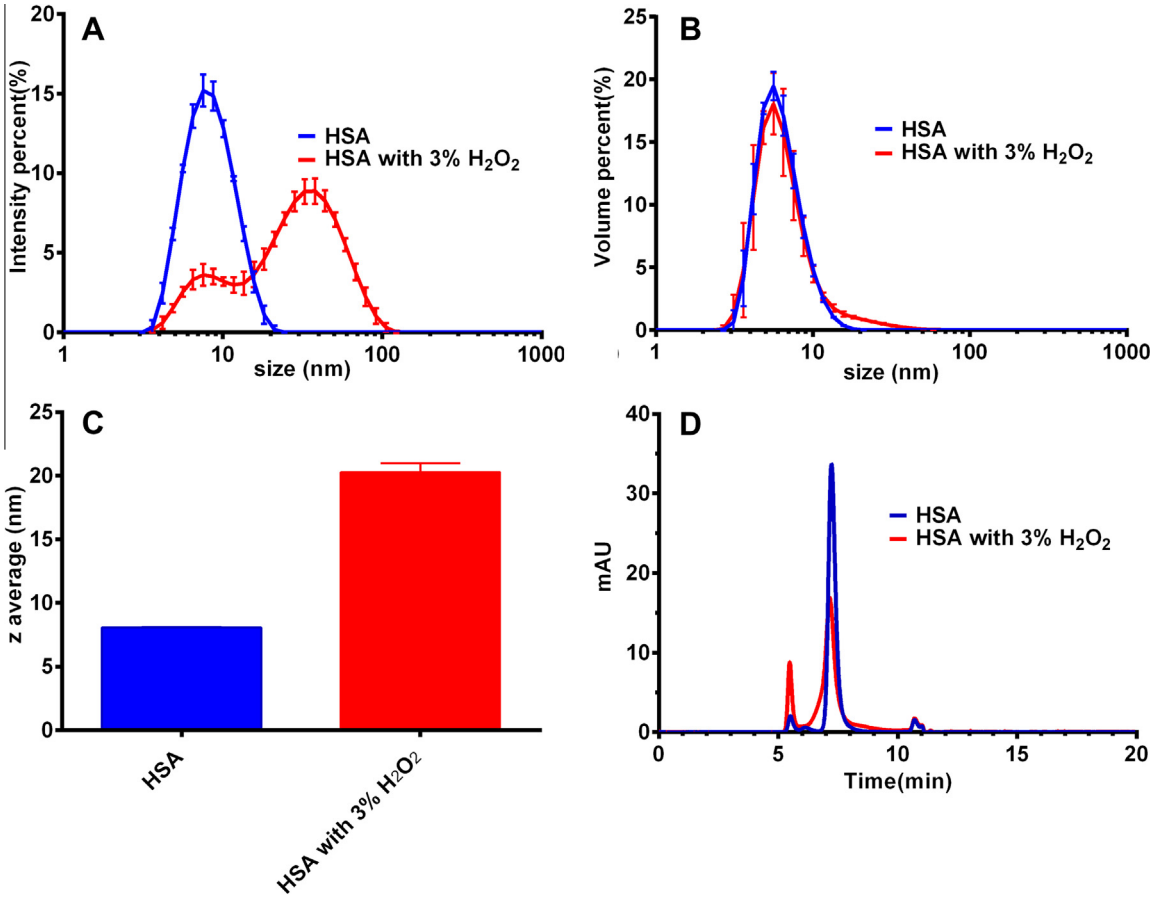

Fig.8. Effects of incubation at 37 °C, with and without 3% H_2O_2 (v/v), on HSA (18 mg/ml) size. (A) DLS intensity distribution. (B) DLS volume distribution. (C) DLS *z*-averaged hydrodynamic size. (D) SEC chromatograms. In panels A, B, and C, error bars denote standard deviations for values obtained for three independent incubated samples.

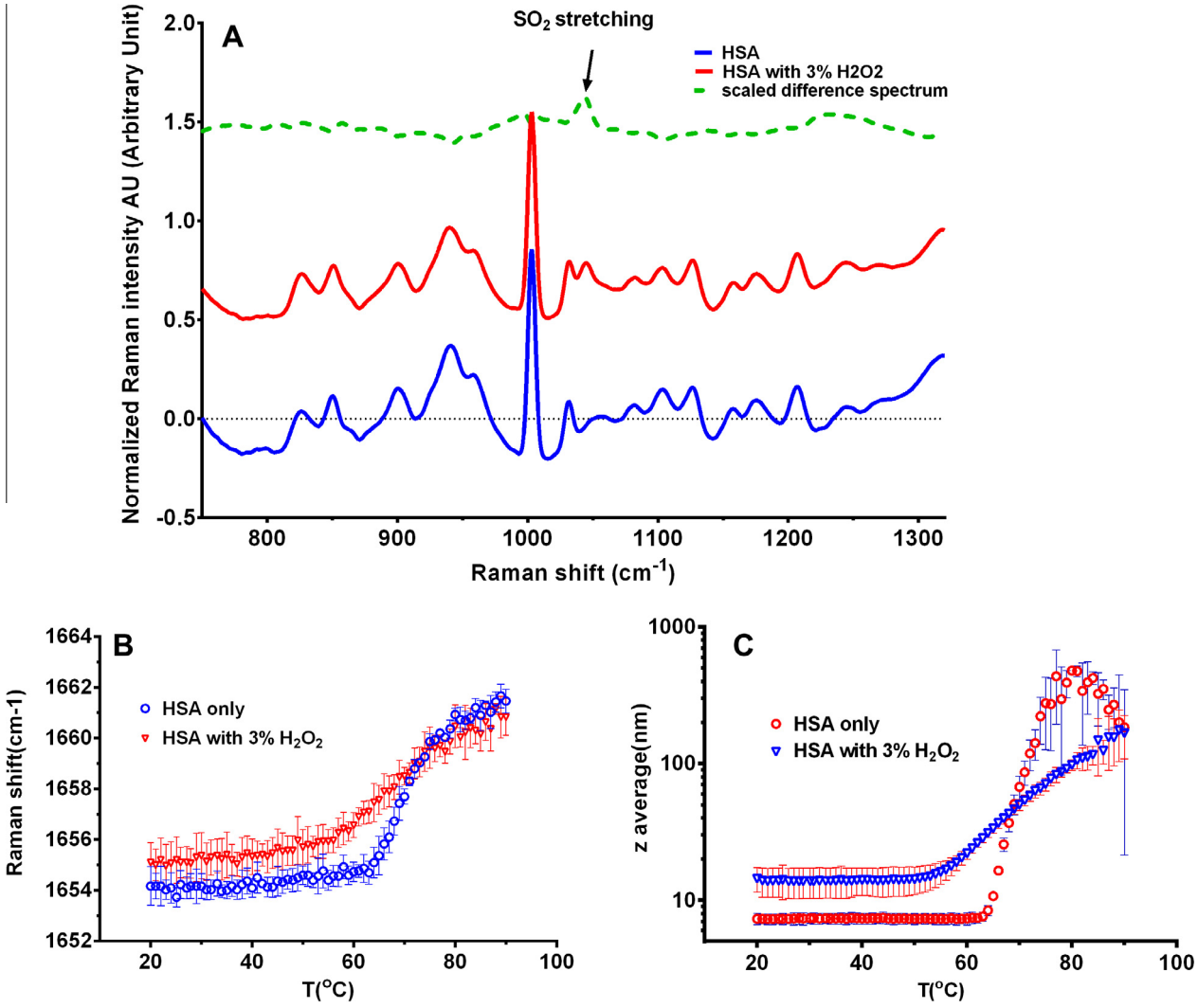

Fig.9. (A) Raman spectra acquired at 20 °C (~800–1300 cm^{-1}) of 18 mg/ml HSA with and without H_2O_2 treatment. The scaled difference spectrum is also shown. The SO_2 stretching reflected by the increase of intensity at 1045 cm^{-1} is labeled in the figures. The spectra are the averages of triplicate samples. (B) Shifting of amide I peak centers of HSA with and without H_2O_2 treatment during thermal ramping. (C) The *z*-averaged hydrodynamic size of HSA with and without H_2O_2 treatment during thermal ramping. Error bars denote standard deviations of three independent samples.

Before evaluation of the thermal stability of H_2O_2-treated HSA, the aggregates formed during the 5-day incubation were removed by preparative ultracentrifugation. The control sample was also processed by ultracentrifugation. The protein concentrations in the supernatants of both samples were adjusted to 18 mg/ml, and thermal stability was studied with Raman spectroscopy and DLS (Fig. 9B and C). As observed in our earlier experiment (Fig. 4A), the amide I peak position for control untreated HSA started from 1654 cm^{-1} at 20 °C and shifted up to 1662 cm^{-1} at 90 °C. With the H_2O_2-treated sample, the peak center was approximately 1655 cm^{-1} at 20 °C, and the final peak position was 1662 cm^{-1} at 90 °C. With H_2O_2-treated HSA, there was a gradual transition during heating rather than the sharp one noted for temperature-dependent peak position for the untreated HSA sample. H_2O_2-treated samples had lower T_{onset} and T_m values than the untreated protein (Table 1), indicating that oxidation reduced thermal stability. Similarly, by DLS, H_2O_2-treated HSA showed a lower T_{agg} value as compared with that for untreated HSA (Table 1).

It should be noted that, even after ultracentrifugation to remove the aggregates of HSA formed during H_2O_2 treatment, the hydrodynamic diameter determined from DLS was approximately 14 nm compared with 7 nm for the control sample of HSA. The presence of residual aggregates, as well as oxidized HSA molecules, in the treated sample might have contributed to the greater hydrodynamic diameter and lower thermal stability. In an earlier study [47], however, based on Rayleigh light scattering intensity, oxidized HSA had a lower aggregation propensity during heating than untreated HSA. The discrepancy between our results and those from the earlier study might be because in our experiment the HSA was stressed with H_2O_2 longer and at higher temperature (37 °C for 5 days vs. 25 °C for 1 day). In addition, the protein concentration in our experiment was 46 mg/ml versus 2 mg/ml in the earlier study. These differences in results between the two studies further illustrate that one cannot assume that similar effects will be observed during heating studies unless all conditions are exactly matched between experiments.

Thermal stability of IVIG

Monoclonal antibodies have become one of the most important categories of therapeutic proteins, and evaluation of thermal stability is crucial for research and development of antibody therapeutic products [51,52]. Because these products are often used at relatively high doses when delivered by subcutaneous

administration, the protein concentration in mAb products can be 50 to 100 mg/ml or maybe even higher. And for thermal stability assessment, it is important to study protein samples at the high concentrations used for the actual dosage form.

To mimic such studies, we examined the thermal stability of an ultracentrifuged IVIG sample at 51 mg/ml by Raman spectroscopy and DLS. The protein solution was prepared in the commercial product formulation of 250 mM glycine buffer at pH 5. The Raman spectra at 20, 60, and 90 °C were selected for initial comparison (Fig. 10). In contrast to results with HSA, which has mostly native α-helix structure, there were minimal temperature-induced shifts in the amide I peak position for the spectra of IVIG at 20 to 90 °C (Figs. 10 and 11A). For the IVIG sample, the amide I band was slightly broadened and the center of the amide I peak shifted slightly from 1668.4 to 1669.8 cm^{-1}. PLS analysis of overall secondary structure of IVIG at 90 °C did show an approximately 5% increase in β-sheet structure. This was far lower than the 40% increase observed for HSA. Antibodies have mostly β-sheet native secondary structure. Therefore, formation of intermolecular β-sheet during protein aggregation was not expected to result in as much increase in overall β-sheet content measured with Raman spectroscopy as that observed with HSA. In addition, with Raman spectroscopy, we were not able to distinguish intermolecular β-sheet in aggregated IVIG from intramolecular β-sheet in the native protein.

Considering the limited resolution with individual spectra for detecting the secondary structural transition of IVIG during heating, we determined difference spectra by subtracting the spectrum obtained at 20 °C from those for the protein at different temperatures during heating (Fig. 11B). With this approach we were able to resolve increased intensities in bands at 1668 and 1686 cm^{-1} with increased temperature (Fig. 11C). Difference spectra provided a sensitive means by which to detect the small increases in β-sheet content in the IVIG sample during heating studies and might be particularly useful for studying mAb therapeutic products.

Assessment of tertiary structure during heating also improved the resolution of structural changes detected with Raman spectroscopy. During heating of IVIG, the Raman spectra showed substantial peak shifts for the tyrosine Fermi doublet at 850 and 830 cm^{-1} and tryptophan at 1550 cm^{-1} (Fig. 10, inset). There was an approximately 2 cm^{-1} reduction in peak positions for the Tyr 850 and 830 cm^{-1} peaks. The Trp 1550 cm^{-1} peak downshifted at around 3 cm^{-1}. Those peak shifts were caused by changes of the local environment of Tyr and Trp, consistent with tertiary structural alterations of IVIG during heating [13]. The T_{onset} and T_m values were determined for Tyr 830 cm^{-1}, Tyr 850 cm^{-1}, and Trp 1550 cm^{-1}, as shown in Table 1. In addition, the intensity ratio of the Fermi doublet of Trp at 1360 and 1340 cm^{-1}, another tertiary structure marker for proteins [13], went from 0.3 to 0.05 (data not shown), with the T_{onset} at 62.7 ± 1.2 °C and T_m at 68.1 ± 0.9 °C (Table 1).

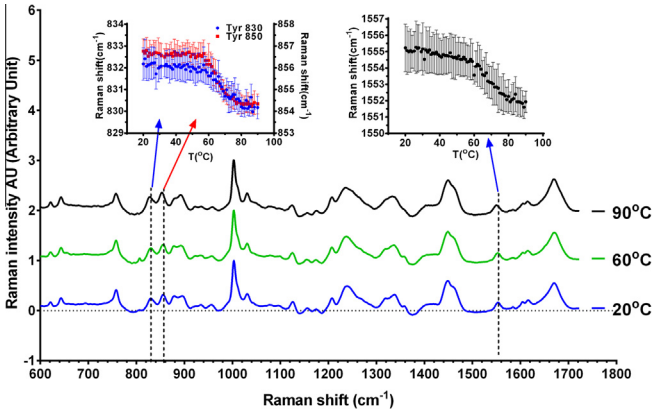

Fig.10. Comprehensive analysis of Raman spectra of 51 mg/ml IVIG during thermal ramping from 20 to 90 °C. Spectra at 20, 60, and 90 °C are selectively shown for comparison. The vertical dashed lines were drawn to highlight the changes of characteristic Raman bands along with the change of temperature. The peak shifting of Tyr 850 and 830 cm^{-1} is shown in the upper left inset, and the peak shifting of Trp 1550 cm^{-1} is shown in the upper right inset. Error bars denote standard deviations of three independent samples.

In an earlier study, second-derivative UV spectra and intrinsic fluorescence spectroscopy of mAb samples also indicated that Trp had increased solvent exposure with increasing temperature [53]. As shown in our work and the earlier study, changes in tertiary structure could be especially valuable to understand mAb structure and thermal stability under circumstances where minimal secondary structure changes occur [54].

Based on the concomitant DLS analysis in our study of IVIG, aggregation was initiated at approximately 56 °C and proceeded further as the temperature increased to form large assemblies of more than 100 nm at 90 °C (Fig. 12A and B). The initial apparent hydrodynamic diameter was 3.5 nm at 20 °C as compared with typical mAb size of approximately 10 nm [55], which is most likely due to the solution conditions employed and the relatively high concentration of IVIG in the sample. The macromolecule concentration effect on molecular diffusion has been developed as [56]

$$D_m = D_0[1 + K_D C + K_2 C^2 + \ldots], \quad (2)$$

where D_m is the mutual diffusion coefficient or the apparent diffusion coefficient, D_o is the value of D_m at infinite dilution, K_D is the first-order interaction parameter, K_2 is the second-order interaction parameter, and C is the protein concentration. At relatively low protein concentration, the higher order concentration effect, K_2, and above are negligible, and the first-order interaction parameter, K_D, could be measured by the correlation between diffusion coefficient and protein concentration to reflect the extent of intermolecular interaction [57]. For example, the apparent diffusion coefficient of a mAb (pI = 8.5) measured with DLS increased almost linearly with an increase in protein concentration in the range of 2 to 12 mg/ml at pHs 4 and 6 [58]. At pHs 4 and 6, the net positive charge on the mAb molecule dominates intermolecular interactions, and the repulsive interaction causes the positive correlation of D_m to protein concentration (or positive K_D) [58]. At higher protein concentration, not only electrostatic interactions but also factors such as van der Waals interactions and excluded volume effects should be considered [59]. In our study, with the pI of immunoglobulin G (IgG) molecules in IVIG ranging from approximately pH 4.7 to 7.5 [22], the majority of the IgG population should be positively charged at pH 5. Therefore, repulsive interactions between the positively charged molecules and an increased diffusion coefficient is expected with increasing protein concentration. In fact, an increase in the apparent diffusion coefficient was seen when the IVIG protein concentration was increased from 1 to 50 mg/ml (data not shown), and the apparent size of IVIG decreased from 9 to 3.4 nm. However, this underestimation of molecular size should not affect aggregation onset point determinations because these values depend on the relative size change rather than the absolute size.

Usually, high-concentration mAb formulations pose challenges for analytical characterization and formulation development. Attempts have been made to obtain analytical data of highly concentrated solutions of mAbs, either solely by infrared spectroscopy [60] or with infrared spectroscopy combined with a series of slightly modified biophysical methods [53,61]. For the former, the thermal stability of bovine IgG was tested up to 200 mg/ml at varied pH values. For the latter, fluorescence, UV, CD, and infrared spectroscopies and DSC were combined to test the effects of pH on the thermal

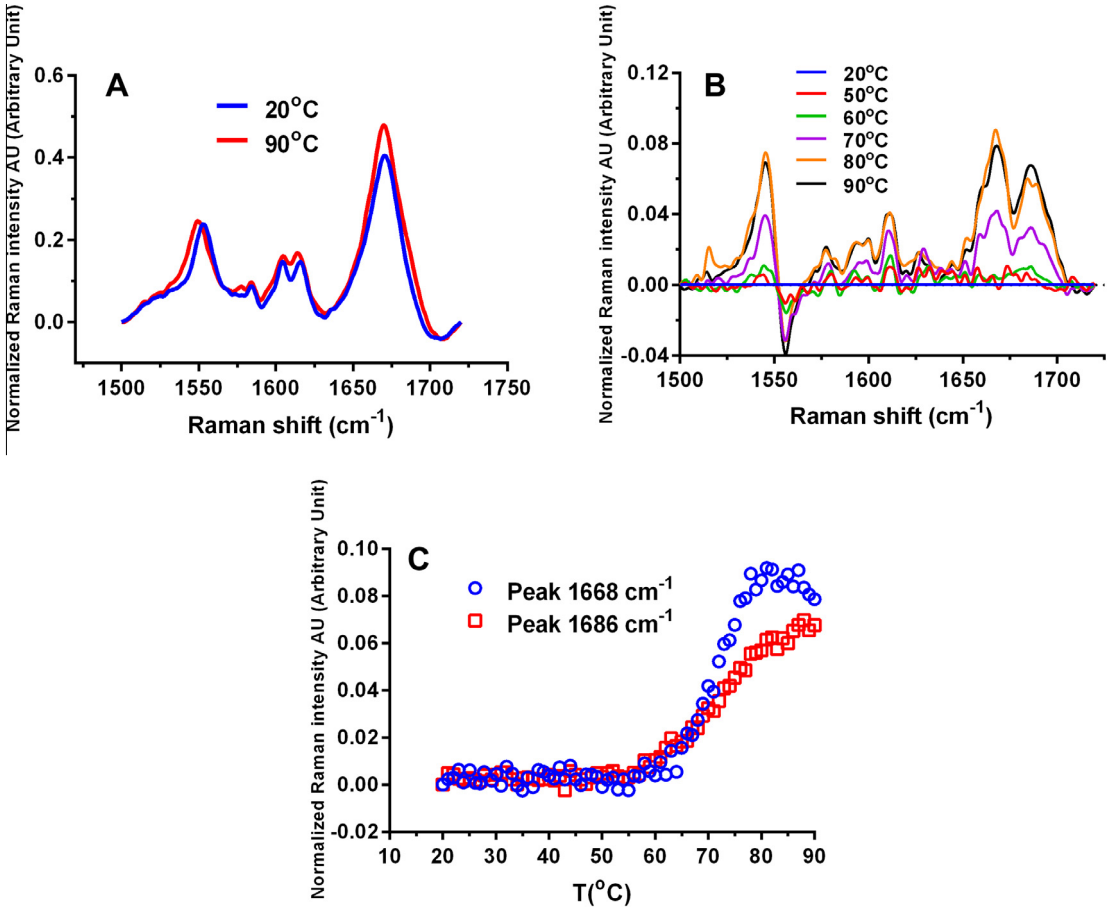

Fig.11. (A) Amide I region in the Raman spectra for IVIG acquired at 20 and 90 °C during heating. (B) Difference spectra in the amide I region obtained by subtracting the Raman spectrum at 20 °C from those acquired during heating at the designated temperatures. (C) Intensities of bands at 1668 and 1686 cm^{-1} in the difference spectra as a function of temperature.

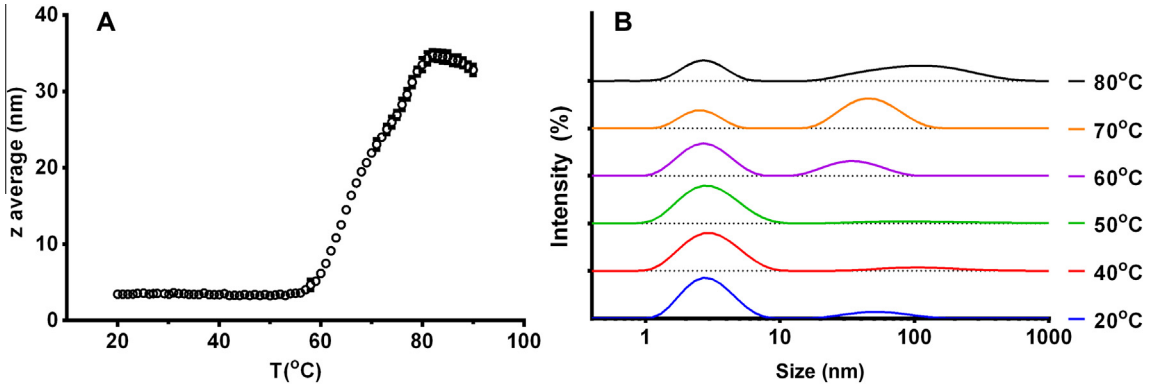

Fig.12. (A) The *z*-averaged hydrodynamic size of IVIG during heating. (B) DLS intensity distributions of IVIG at 20, 40, 50, 60, 70, and 80 °C. In panel A, error bars denote standard deviations of values obtained for three independent samples.

stability of two mAbs across a concentration range of 0.1 to 190 mg/ml. Interestingly, at pH 6, the bovine IgG was found to have increasing T_m values from 71 to 73 °C when the protein concentration increased from 25 to 100 mg/ml, but the value decreased slightly at 200 mg/ml. However, for the study of the two mAbs, spectroscopic techniques probing tertiary structure demonstrated a decrease in the apparent thermal melting temperature of approximately 5 to 20 °C with increasing protein concentration. In these two studies, the apparent melting temperature decrement was attributed to increased aggregation at higher protein concentration. However, no direct size measurements were performed. Conversely in another recent study, only light scattering was applied to characterize protein aggregation at concentration up to 190 mg/ml, but no structure information was supplied [61]. In contrast, with the combined DLS–Raman system, both protein conformational and aggregation can be studied at the same time.

Conclusions

The combination of Raman spectroscopy and DLS offers unique advantages such as low sample volume requirement, easy background subtraction, compatibility with high protein concentration,

and simultaneous analysis for both size and conformation, including protein secondary and tertiary structure information. The robustness of a combined Raman–DLS system for protein thermal stability evaluations has been documented by the current study, and further applications of this system for other protein systems will be forthcoming.

Acknowledgment

We thank Malvern Bioscience Development Initiative for providing the instrument and financial support for this work.

Appendix A. Supplementary data

Supplementary data associated with this article can be found, in the online version, at http://dx.doi.org/10.1016/j.ab.2014.11.016.

References

[1] L.O. Narhi, Y. Jiang, R. Deshpande, S. Kang, J. Shultz, Approaches to control protein aggregation during bulk production, in: W. Wang, C.J. Roberts (Eds.), Aggregation of Therapeutic Proteins, John Wiley, New York, 2010, pp. 257–299.
[2] T. Wang, O.S. Kumru, L. Yi, Y.J. Wang, J. Zhang, J.H. Kim, S.B. Joshi, C.R. Middaugh, D.B. Volkin, Effect of ionic strength and pH on the physical and chemical stability of a monoclonal antibody antigen-binding fragment, J. Pharm. Sci. 102 (2013) 2520–2537.
[3] J. Liu, C.A. Blasie, S. Shi, S.B. Joshi, C.R. Middaugh, D.B. Volkin, Characterization and stabilization of recombinant human protein pentraxin (rhPTX-2), J. Pharm. Sci. 102 (2013) 827–841.
[4] M.A. Alsenaidy, N.K. Jain, J.H. Kim, C.R. Middaugh, D.B. Volkin, Protein comparability assessments and potential applicability of high throughput biophysical methods and data visualization tools to compare physical stability profiles, Front. Pharmacol. 5 (2014) 39.
[5] M. Federici, A. Lubiniecki, P. Manikwar, D.B. Volkin, Analytical lessons learned from selected therapeutic protein drug comparability studies, Biologicals 41 (2013) 131–147.
[6] A. Lubiniecki, D.B. Volkin, M. Federici, M.D. Bond, M.L. Nedved, L. Hendricks, P. Mehndiratta, M. Bruner, S. Burman, P. Dalmonte, J. Kline, A. Ni, M.E. Panek, B. Pikounis, G. Powers, O. Vafa, R. Siegel, Comparability assessments of process and product changes made during development of two different monoclonal antibodies, Biologicals 39 (2011) 9–22.
[7] A. Hawe, M. Wiggenhorn, M. van de Weert, J.H. Garbe, H.C. Mahler, W. Jiskoot, Forced degradation of therapeutic proteins, J. Pharm. Sci. 101 (2012) 895–913.
[8] J.S. Philo, A critical review of methods for size characterization of non-particulate protein aggregates, Curr. Pharm. Biotechnol. 10 (2009) 359–372.
[9] J.G. Barnard, S. Singh, T.W. Randolph, J.F. Carpenter, Subvisible particle counting provides a sensitive method of detecting and quantifying aggregation of monoclonal antibody caused by freeze–thawing: insights into the roles of particles in the protein aggregation pathway, J. Pharm. Sci. 100 (2011) 492–503.
[10] S. Zolls, R. Tantipolphan, M. Wiggenhorn, G. Winter, W. Jiskoot, W. Friess, A. Hawe, Particles in therapeutic protein formulations: 1. Overview of analytical methods, J. Pharm. Sci. 101 (2012) 914–935.
[11] S.K. Singh, M.R. Toler, Monitoring of subvisible particles in therapeutic proteins, Methods Mol. Biol. 899 (2012) 379–401.
[12] H.C. Mahler, W. Friess, U. Grauschopf, S. Kiese, Protein aggregation: pathways, induction factors, and analysis, J. Pharm. Sci. 98 (2009) 2909–2934.
[13] Z.Q. Wen, Raman spectroscopy of protein pharmaceuticals, J. Pharm. Sci. 96 (2007) 2861–2878.
[14] A. Hedoux, Y. Guinet, L. Paccou, Analysis of the mechanism of lysozyme pressure denaturation from Raman spectroscopy investigations, and comparison with thermal denaturation, J. Phys. Chem. B 115 (2011) 6740–6748.
[15] G. Navarra, A. Tinti, M. Leone, V. Militello, A. Torreggiani, Influence of metal ions on thermal aggregation of bovine serum albumin: aggregation kinetics and structural changes, J. Inorg. Biochem. 103 (2009) 1729–1738.
[16] V.L. Brewster, L. Ashton, R. Goodacre, Monitoring guanidinium-induced structural changes in ribonuclease proteins using Raman spectroscopy and 2D correlation analysis, Anal. Chem. 85 (2013) 3570–3575.
[17] S. Ikeda, E.C.Y. Li-Chan, Raman spectroscopy of heat-induced fine-stranded and particulate β-lactoglobulin gels, Food Hydrocolloids 18 (2004) 489–498.
[18] A.C. Dong, B. Kendrick, L. Kreilgard, J. Matsuura, M.C. Manning, J.F. Carpenter, Spectroscopic study of secondary structure and thermal denaturation of recombinant human factor XIII in aqueous solution, Arch. Biochem. Biophys. 347 (1997) 213–220.
[19] V. Kumar, N. Dixit, L.L. Zhou, W. Fraunhofer, Impact of short range hydrophobic interactions and long range electrostatic forces on the aggregation kinetics of a monoclonal antibody and a dual-variable domain immunoglobulin at low and high concentrations, Int. J. Pharm. 421 (2011) 82–93.
[20] E. N. Lewis, Malvern Instruments, Dual-mode characterization of particulates, patent WO/2013/027034 (2013).
[21] S. Muzammil, Y. Kumar, S. Tayyab, Erratum [Molten globule-like state of human serum albumin at low pH, 266, pp. 26–34, 1999], Eur. J. Biochem. 267 (2000) 1261.
[22] A. Szenczi, J. Kardos, G.A. Medgyesi, P. Zavodszky, The effect of solvent environment on the conformation and stability of human polyclonal IgG in solution, Biologicals 34 (2006) 5–14.
[23] T. Rispens, C.M. Lakemond, N.I. Derksen, R.C. Aalberse, Detection of conformational changes in immunoglobulin G using isothermal titration calorimetry with low-molecular-weight probes, Anal. Biochem. 380 (2008) 303–309.
[24] C. David, S. Foley, C. Mavon, M. Enescu, Reductive unfolding of serum albumins uncovered by Raman spectroscopy, Biopolymers 89 (2008) 623–634.
[25] X.C. Shen, H. Liang, J.H. Guo, C. Song, X.W. He, Y.Z. Yuan, Studies on the interaction between Ag(+) and human serum albumin, J. Inorg. Biochem. 95 (2003) 124–130.
[26] A. Saha, V.V. Yakovlev, Structural changes of human serum albumin in response to a low concentration of heavy ions, J. Biophotonics 3 (2010) 670–677.
[27] A. Hedoux, L. Paccou, S. Achir, Y. Guinet, In situ monitoring of proteins during lyophilization using micro-Raman spectroscopy: a description of structural changes induced by dehydration, J. Pharm. Sci. 101 (2012) 2316–2326.
[28] A.I. Ivanov, R.G. Zhbankov, E.A. Korolenko, E.V. Korolik, L.A. Meleshchenko, M. Marchewka, H. Ratajczak, Infrared and Raman spectroscopic studies of the structure of human serum albumin under various ligand loads, J. Appl. Spectrosc. 60 (1994) 305–309.
[29] S.U. Sane, S.M. Cramer, T.M. Przybycien, A holistic approach to protein secondary structure characterization using amide I band Raman spectroscopy, Anal. Biochem. 269 (1999) 255–272.
[30] X.M. He, D.C. Carter, Atomic structure and chemistry of human serum albumin, Nature 358 (1992) 209–215.
[31] L. Galantini, C. Leggio, N.V. Pavel, Human serum albumin unfolding: a small-angle X-ray scattering and light scattering study, J. Phys. Chem. B 112 (2008) 15460–15469.
[32] B.S. Kendrick, J.L. Cleland, X. Lam, T. Nguyen, T.W. Randolph, M.C. Manning, J.F. Carpenter, Aggregation of recombinant human interferon gamma: kinetics and structural transitions, J. Pharm. Sci. 87 (1998) 1069–1076.
[33] M. Bouchard, J. Zurdo, E.J. Nettleton, C.M. Dobson, C.V. Robinson, Formation of insulin amyloid fibrils followed by FTIR simultaneously with CD and electron microscopy, Protein Sci. 9 (2000) 1960–1967.
[34] A. Natalello, D. Ami, S. Brocca, M. Lotti, S.M. Doglia, Secondary structure, conformational stability, and glycosylation of a recombinant *Candida rugosa* lipase studied by Fourier-transform infrared spectroscopy, Biochem. J. 385 (2005) 511–517.
[35] F. Meilleur, J. Contzen, D.A. Myles, C. Jung, Structural stability and dynamics of hydrogenated and perdeuterated cytochrome P450cam (CYP101), Biochemistry 43 (2004) 8744–8753.
[36] K. Wallevik, Reversible denaturation of human serum albumin by pH, temperature, and guanidine hydrochloride followed by optical rotation, J. Biol. Chem. 248 (1973) 2650–2655.
[37] G.A. Pico, Thermodynamic features of the thermal unfolding of human serum albumin, Int. J. Biol. Macromol. 20 (1997) 63–73.
[38] B. Farruggia, G.A. Pico, Thermodynamic features of the chemical and thermal denaturations of human serum albumin, Int. J. Biol. Macromol. 26 (1999) 317–323.
[39] K. Flora, J.D. Brennan, G.A. Baker, M.A. Doody, F.V. Bright, Unfolding of acrylodan-labeled human serum albumin probed by steady-state and time-resolved fluorescence methods, Biophys. J. 75 (1998) 1084–1096.
[40] A.K. Shaw, S.K. Pal, Spectroscopic studies on the effect of temperature on pH-induced folded states of human serum albumin, J. Photochem. Photobiol., B 90 (2008) 69–77.
[41] R. Torosantucci, C. Schoneich, W. Jiskoot, Oxidation of therapeutic proteins and peptides: structural and biological consequences, Pharm. Res. 31 (2014) 541–553.
[42] D.K. Chou, Mechanistic Insights into Physical and Chemical Stability of Albumin Fusion Proteins in Aqueous Solution, University of Colorado Health Sciences Center, Aurora, CO, 2008.
[43] D. Liu, D. Ren, H. Huang, J. Dankberg, R. Rosenfeld, M.J. Cocco, L. Li, D.N. Brems, R.L. Remmele Jr., Structure and stability changes of human IgG_1 Fc as a consequence of methionine oxidation, Biochemistry 47 (2008) 5088–5100.
[44] W. Burkitt, P. Domann, G. O'Connor, Conformational changes in oxidatively stressed monoclonal antibodies studied by hydrogen exchange mass spectrometry, Protein Sci. 19 (2010) 826–835.
[45] D. Houde, Y. Peng, S.A. Berkowitz, J.R. Engen, Post-translational modifications differentially affect IgG_1 conformation and receptor binding, Mol. Cell. Proteomics 9 (2010) 1716–1728.
[46] F. Mulinacci, E. Poirier, M.A. Capelle, R. Gurny, T. Arvinte, Influence of methionine oxidation on the aggregation of recombinant human growth hormone, Eur. J. Pharm. Biopharm. 85 (2013) 42–52.
[47] G. Sancataldo, V. Vetri, V. Fodera, G. Di Cara, V. Militello, M. Leone, Oxidation enhances human serum albumin thermal stability and changes the routes of amyloid fibril formation, PLoS ONE 9 (2014) e84552.
[48] H. Rokos, J. Moore, S. Hasse, J.M. Gillbro, J.M. Wood, K.U. Schallreuter, In vivo fluorescence excitation spectroscopy and in vivo Fourier-transform Raman

spectroscopy in human skin: evidence of H_2O_2 oxidation of epidermal albumin in patients with vitiligo, J. Raman Spectrosc. 35 (2004) 125–130.
[49] N.C. Gibbons, J.M. Wood, H. Rokos, K.U. Schallreuter, Computer simulation of native epidermal enzyme structures in the presence and absence of hydrogen peroxide (H_2O_2): potential and pitfalls, J. Invest. Dermatol. 126 (2006) 2576–2582.
[50] A. Torreggiani, S. Barata-Vallejo, C. Chatgilialoglu, Combined Raman and IR spectroscopic study on the radical-based modifications of methionine, Anal. Bioanal. Chem. 401 (2011) 1231–1239.
[51] S. Goswami, W. Wang, T. Arakawa, S. Ohtake, Developments and challenges for mAb-based therapeutics, Antibodies 2 (2013) 452–500.
[52] W. Wang, S. Singh, D.L. Zeng, K. King, S. Nema, Antibody structure, instability, and formulation, J. Pharm. Sci. 96 (2007) 1–26.
[53] N. Harn, C. Allan, C. Oliver, C.R. Middaugh, Highly concentrated monoclonal antibody solutions: direct analysis of physical structure and thermal stability, J. Pharm. Sci. 96 (2007) 532–546.
[54] R. Paul, A. Graff-Meyer, H. Stahlberg, M.E. Lauer, A.C. Rufer, H. Beck, A. Briguet, V. Schnaible, T. Buckel, S. Boeckle, Structure and function of purified monoclonal antibody dimers induced by different stress conditions, Pharm. Res. 29 (2012) 2047–2059.
[55] U. Nobbmann, M. Connah, B. Fish, P. Varley, C. Gee, S. Mulot, J. Chen, L. Zhou, Y. Lu, F. Shen, J. Yi, S.E. Harding, Dynamic light scattering as a relative tool for assessing the molecular integrity and stability of monoclonal antibodies, Biotechnol. Genet. Eng. Rev. 24 (2007) 117–128.
[56] S. Li, D. Xing, J. Li, Dynamic light scattering application to study protein interactions in electrolyte solutions, J. Biol. Phys. 30 (2004) 313–324.
[57] S. Saito, J. Hasegawa, N. Kobayashi, N. Kishi, S. Uchiyama, K. Fukui, Behavior of monoclonal antibodies: relation between the second virial coefficient (B_2) at low concentrations and aggregation propensity and viscosity at high concentrations, Pharm. Res. 29 (2012) 397–410.
[58] S. Yadav, S.J. Shire, D.S. Kalonia, Viscosity behavior of high-concentration monoclonal antibody solutions: correlation with interaction parameter and electroviscous effects, J. Pharm. Sci. 101 (2012) 998–1011.
[59] S. Yadav, J. Liu, S.J. Shire, D.S. Kalonia, Specific interactions in high concentration antibody solutions resulting in high viscosity, J. Pharm. Sci. 99 (2010) 1152–1168.
[60] V. Sathya Devi, D.R. Coleman, J. Truntzer, Thermal unfolding curves of high concentration bovine IgG measured by FTIR spectroscopy, Protein J. 30 (2011) 395–403.
[61] M.F. Drenski, M.L. Brader, R.W. Alston, W.F. Reed, Monitoring protein aggregation kinetics with simultaneous multiple sample light scattering, Anal. Biochem. 437 (2013) 185–197.